Studies on Corrosion Behavior of 6061 Al-15 vol. pct. $SiC_{(p)}$ Composite in HCl Medium by Electrochemical Techniques

K. S. Shetty, A. N. Shetty*

Department of Chemistry
National Institute of Technology Karnataka, Surathkal, Srinivasnagar-575025, Karnataka, India,
**e-mail: nityashreya@gmail.com*

The micro-galvanic corrosion of SiC reinforced 6061 Al alloys deprives its potential application in the acidic conditions or at high temperatures. Therefore, the corrosion behavior of 6061 Al-15 vol.pct. $SiC_{(p)}$ composite in HCl medium at different temperatures was studied using electrochemical impedance measurements and potentiodynamic polarization curves. The studies revealed that, on increasing the ionic concentration of the medium and temperature the rate of corrosion also increases. Scanning electron microscopic imaging of polished and immersed sample in the medium showed the smooth and uneven morphology respectively. Activation parameters like energy of activation was calculated from Arrhenius plots. Entropy and enthalpy values were derived from the plots of transition state theory equation.

Keywords: 6061 Al composite, electrochemical techniques, acidic corrosion, silicon carbide reinforcement.

УДК 620.193.4:544.6

INTRODUCTION

Aluminum, being world's third most abundant element, is associated with the distinguishable properties like strength, lightness, recyclability, formability, corrosion resistance, etc. [1–3]. However, to ameliorate the performance and to boost the strength to weight ratio they are more often reinforced with ceramic SiC particulate matter and transformed into composites [4–6]. The properties of aluminum composites, such as greater stiffness, reduced coefficient of thermal expansion, etc., make it exceedingly advantageous in applications like parts of aircrafts, building materials, architectural designs and also in food and packaging industries [7–9]. Although one can witness wide array of applications of aluminum composites, the common problem encountered is the lower corrosion resistant properties exhibited by them. The main reason behind this could be attributed to the discontinuity of the surface protective oxide film after reinforcement of ceramic SiC particles [10–11]. Semi-conducting behavior of SiC particles make them to act as efficient cathodic sites which enhances micro-galvanic corrosion [12–14]. The Corrosion behavior of composites are governed by processing techniques, type of reinforcement and particle size and are specific to individual composites. Therefore it results in insufficient information on the corrosion behavior of composites as the results are not comparable. The high temperature applications of composites comprises brake rotors of vehicles, drive shafts, etc. The surface preparation of metals for electroplating techniques involve acid cleaning, scouring and so on [15–17]. The effect of such processes leads to corrosion, which in turn may cause undesirable effects on the functioning and applications of the material. Severe pitting attack of these composites in the presence of highly aggressive anions like chloride ion for pure aluminum and its alloys have been reported [18–19]. However, a detailed electrochemical investigation on corrosion behavior of 6061 Al-15 vol. pct. $SiC_{(p)}$ composite in hydrochloric acid medium in particular, seldom appears in the literature. Consequently, the present research work was carried out to make a methodical study of the corrosion behavior of 6061 Al-15 vol. pct. $SiC_{(p)}$ composite in varied concentrations of hydrochloric acid medium and also at different temperatures.

EXPERIMENTAL

Material

Experiments were carried out using the 6061 Al-15 vol.pct. $SiC_{(p)}$ composite, supplied by NIIST Trivandrum, India. The specimen was used in the extruded rod form, whose extrusion ratio is 30:1. Table 1 gives the composition of the 6061 Al alloy, as given by the supplier. The cylindrical test coupon, obtained from the rod was molded with epoxy resin, exposing a constant area of 1.102 cm^2 of the sample to the electrolyte media. The test coupons polished as per the metallographic practices. The coupon was subjected to belt grinding first, followed with polishing with different grades of emery papers, ranging from rough to smooth grades, and finally the surface is mirror finished by disc polishing using legated alumina. After cleaning with double distilled water and acetone, the test coupons were dried and immediately used for electrochemical analysis.

© Shetty K.S., Shetty A.N., Электронная обработка материалов, 2015, **51**(4), 68–75.

Table 1. Composition of the base metal Al 6061 alloy

Element	Cu	Cr	Si	Mg	Al
Composition (wt. %)	0.25	0.25	0.6	1.0	97.9

Medium

The electrolyte media of total five different concentrations 0.025M, 0.05M, 0.1M, 0.125M, and 0.25M were prepared by the stock dilution of 1M hydrochloric acid in double distilled water. Each of the solutions were titrated against sodium carbonate which is a primary standard to get accurate concentration using methyl orange as an indicator.

Electrochemical Measurements

The electrochemical work station, Gill AC having ACM instrument version 5 software was used to carry out the electrochemical measurements. A conventional three electrode Pyrex glass cell was used with the molded test coupon acting as a working electrode, the platinum electrode served as an auxiliary electrode, against the saturated calomel electrode (SCE) as the reference electrode. Immediately after the electrochemical impedance studies, test coupon was subjected to potentiodynamic polarization measurements without further surface treatment. The measurements were carried out in HCl media at different temperatures, ranging between 30–50^{o}C.

Potentiodynamic Polarization Studies

The finely polished test coupons were immersed in the acid medium and was allowed to attain steady state open circuit potential (OCP). The potentiodynamic current-potential curves were recorded by polarizing the specimen to -250 mV cathodically and +250 mV anodically with respect to the open circuit potential (OCP) at a scan rate of 1 mV/s.

Electrochemical Impedance Spectroscopy (EIS) Studies

The EIS measurements were carried out by impressing a periodic 10 mV small amplitude of AC signal over a wide frequency spectrum of 100 kHz – 0.01 Hz on the OCP. The impedance data were analyzed by using Nyquist plots.

All the results reported are average of three similar results.

Scanning electron microscopy (SEM) Analysis

JEOL JSM-6380LA model SEM was used to image the surface morphology of the corroded and polished specimen of 6061 Al-15 vol.pct. $SiC_{(p)}$ composite.

RESULTS AND DISCUSSION

Potentiodynamic Polarization Measurements

The potentiodynamic polarization curves were recorded for the corrosion of the composite in different concentrations of hydrochloric acid and at different temperatures. Potentiodynamic polarization curves for the corrosion of the composite sample in different concentrations of HCl at 40°C are shown in Fig. 1. Similar plots were obtained at other temperatures considered. The electrochemical parameters such as corrosion potential (E_{corr}), the corrosion current density (i_{corr}) and the Tafel cathodic slope β_c are tabulated in the Table 2. Owing to the ill-defined anodic current plateau, the i_{corr} values were determined by the extrapolation of linear cathodic part to the respective corrosion potentials alone [20]. The Tafel constants were calculated at 50 mV from the OCP, from slope values obtained by a tangent drawn where the cathodic region remains linear for at least one decade. The anodic region exemplifies the metal oxidation and the cathodic region interprets the evolution of hydrogen in the case of acidic conditions. The rate of corrosion (ν_{corr}) was calculated using equation 1 [21].

$$\nu_{corr} = \frac{K \cdot i_{corr} \cdot E.W}{\rho} \quad (1)$$

where ν_{corr} is the corrosion rate expressed as mm·y^{-1}, K is the proportionality constant = 0.00327, i_{corr} is the corrosion current density in μA·cm^{-2}, $E.W$ is the equivalent weight of the composite, ρ is the density expressed as g·cm^{-3}. The $E.W$ was calculated using equation 2.

$$E.W = \frac{1}{\sum\left(n_i f_i / w_i\right)} \quad (2)$$

where n_i is the valence of the i^{th} element of the alloy, f_i is the weight fraction of the i^{th} element in the alloy and w_i is the atomic weight of the i^{th} element in the alloy.

It may be observed that the corrosion current density and corrosion rate values increase when the concentration of HCl and the temperature are increased. As can be seen from Fig. 1 both the anodic and cathodic polarization curves are shifted towards the higher current density region when the concentration of HCl is increased. This trend implies the fact that the rate of both the anodic and cathodic reactions responsible for the corrosion of the composite sample are affected by the concentration of HCl.

In the presence of HCl, the Cl^- ions are likely to percolate through the oxide film thereby retarding the self-healing ability of the oxide layer on the metal surface. This results in the formation of inter-

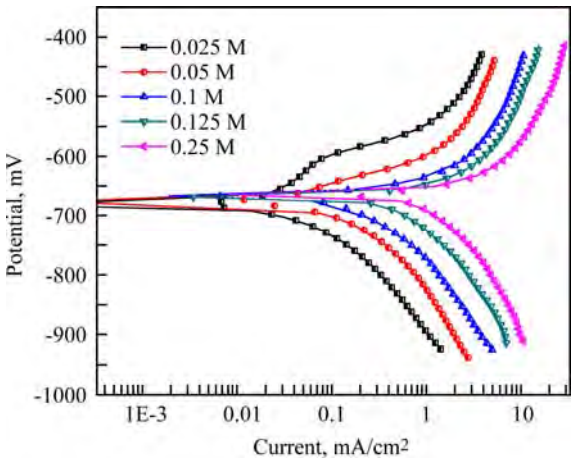

Fig. 1. Potentiodynamic polarization curves for the corrosion of 6061 Al-15 vol. pct. $SiC_{(p)}$ composite in different concentrations of hydrochloric acid at 40°C.

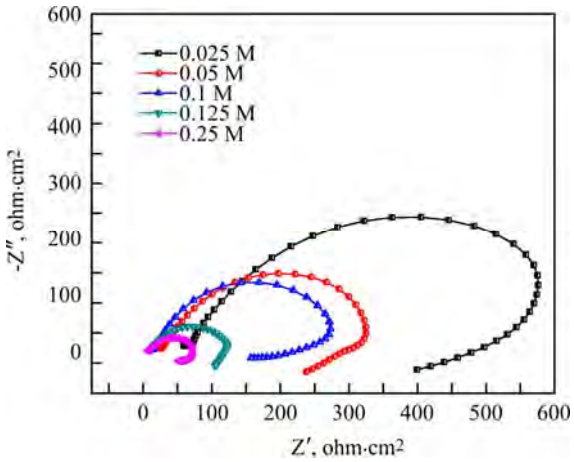

Fig. 2. Nyquist plots for the corrosion of 6061 Al-15 vol. pct $SiC_{(p)}$ composite in different concentrations of hydrochloric acid at 30°C.

Table 2. Potentiodynamic polarization data for the corrosion of 6061 Al-15 vol. pct. $SiC_{(p)}$ composite in hydrochloric acid.

Concentration (M)	Temp (^{0}C)	E_{corr} (mV)	-β_c (mV·dec^{-1})	i_{corr} (μA·cm^{-2})	v_{corr} (mm·y^{-1})
0.025	30	-696.15	215.82	54.63	0.59
	35	-676.98	192.23	102.63	1.10
	40	-693.97	216.08	134.45	1.45
	45	-690.68	225.49	161.74	1.74
	50	-714.11	224.30	180.88	1.95
0.05	30	-666.43	209.23	122.59	1.32
	35	-683.48	207.85	125.68	1.35
	40	-676.98	204.29	191.69	2.06
	45	-686.10	198.35	288.82	3.11
	50	-693.68	217.36	385.91	4.15
0.1	30	-664.80	166.40	150.88	1.62
	35	-659.46	199.00	269.59	2.90
	40	-665.21	188.60	497.58	5.36
	45	-691.22	204.50	726.33	7.82
	50	-702.65	223.52	874.56	9.41
0.125	30	-660.51	270.02	643.35	6.92
	35	-667.24	290.42	679.18	7.31
	40	-667.35	247.53	791.76	8.52
	45	-678.65	321.56	857.07	9.22
	50	-656.99	220.43	978.53	10.53
0.25	30	-658.21	293.79	898.34	9.67
	35	-664.10	224.44	1239.40	13.34
	40	-658.86	308.04	1807.00	19.45
	45	-684.72	277.1	1878.30	20.22
	50	-667.12	246.89	2135.90	22.99

mediate soluble complex as given in the equation 3 below.

$$Al_{(s)} + nCl^- \rightarrow \left[AlCl_n\right]_{(aq)}^{(n-3)} + 3e^-. \qquad (3)$$

The complex thus formed enhances the dissolution of the aluminum ions from the lattice into the solution and leads to local thinning of the passive layer making it pervious for further attack by chloride ions leading to severe pitting attack [16].

The equations (4) and (5) represent the anodic and cathodic reaction in acidic condition. The overall reaction involved in the corrosion reaction of the composite is given in equation (6).

$$\left(Al_{(s)} \rightarrow Al^{3+} + 3e^-\right) \times 2, \qquad (4)$$

$$\left(2H^+ + 2e^- \rightarrow H_2 \uparrow\right) \times 3, \qquad (5)$$

$$2Al_{(s)} + 6H^+ \rightarrow 2Al^{3+} + 3H_2 \uparrow. \qquad (6)$$

Electrochemical Impedance Spectroscopy Measurements

The impedance plots for the corrosion of the composite in different concentrations of hydrochloric acid at 30°C are shown in the Fig. 2. The Nyquist plots presented one high frequency capacitive loop and a low frequency inductive loop. From the semi-circles in the plots it can be inferred that the process of corrosion is largely charge-transfer controlled [22]. A large capacitive loop at high frequency (HF) region and a small inductive loop at lower frequency (LF) region observed in the impedance spectra are consistent with the plots reported in the literature for the corrosion of pure aluminum or aluminum alloys in medium like HCl, H_2SO_4, etc. [23]. The HF capacitive loop indicates the bulk relaxation process of the oxide layer that is present on the surface of aluminum [24]. Additional clarification of the presence of HF capacitive loop is imputed to the oxidation of aluminum at the electrode-electrolyte interface in precise [25]. The LF inductive loop is ascribed to the adsorption and inclusion of the Cl^- and H^+ ions into the oxide film [26]. These data are reliable with the mechanism that proposed the chemisorption of Cl^- ions into the oxide surface forming oxide-chloride complex. Aluminum oxide film is regarded to be a parallel circuit of resistor due to the ionic conduction in the oxide film and a capacitor due to its dielectric properties [22]. For better interpretation of the EIS data, an equivalent circuit displayed as an inset in the Fig. 3, comprising of five circuit elements was derived from the simulation plot shown in the Fig. 3. The equivalent circuit consists of solution resistance (R_s), a constant phase element (Q) that is parallel to the charge transfer resistance (R_{ct}) and inductive resistance (R_L). The R_L is in series with the inductor L. The constant phase element (Q) replaces an ideal capacitor (C) as the nature of semi-circle in the Nyquist plot appears to be depressed. This depression in the plot may be attributed to the inhomogeneity of the solid surface of the composite during reinforcement with SiC particle. Equation 7 gives the expression using which the double layer capacitance may be calculated.

$$C_{dl} = Y_0 \left(2\pi f_{\max}\right)^{n-1}. \tag{7}$$

The exponent n in the equation 3 is the deviation parameter from the ideal capacitor behavior, f_{max} is the frequency at which the imaginary component of the impedance is maximum and Y_0 is the amplitude.

In the presence of inductive loop, the polarization resistance (R_p) was calculated using the formula mentioned in equation 8.

$$R_p = \frac{R_L \times R_{ct}}{R_L + R_{ct}}. \tag{8}$$

Table 3 comprises of the results of EIS, from which it can be interpreted that as the concentration of the acid increases, the value of R_p decreases, which means that the resistance for the process of corrosion is decreased there by enhancing the degree of corrosion. Similar trend was witnessed by the results of potentiodynamic polarization measurements discussed above. EIS results of all other temperatures considered were similar to the one mentioned.

Effect of Temperature

The effect of temperature on the corrosion rate of the composite was assessed by running the EIS and potentiodynamic polarization curves at five different temperatures, starting from 30°C with an increment of 5°C up to 50°C.

The Fig. 4 and Fig. 5 depict the EIS and potentiodynamic polarization plots for the corrosion of the composite at different temperatures in 0.05M HCl and 0.25M HCl, respectively. From Fig. 4 one can infer that as the temperature rises the diameters of the semi-circles, which contribute to the polarization resistance in the impedance plot tend to diminish, indicating the increase in the corrosion rate [27]. Likewise, as seen in Fig. 5 the polarization curves shift to the higher i_{corr} values as the temperature is increased, indicating an increase in the corrosion rate with the increase in temperature. These observations could be attributed to the fact that as the temperature increases the rate of the corrosion reaction increases just as any other chemical or electrochemical reactions. Arrhenius equation 9 was used to calculate the energy of activation (E_a) for the corrosion reaction.

$$\nu_{corr} = Ae^{-Ea/RT} \tag{9}$$

where A in the equation is a constant and R is the ideal gas constant. The Arrhenius plots for the corrosion of the composite in HCl medium of different concentrations are presented in Fig. 6. The activation energies were calculated using the slope obtained from linear fit of the plot [28].

The enthalpy of activation ($\Delta H^{\#}$) and entropy of activation ($\Delta S^{\#}$) were calculated from the transition state theory equation 10.

$$\nu_{corr} = \frac{RT}{Nh} e^{\Delta S^{\#}/R} e^{-\Delta H^{\#}/RT} \tag{10}$$

where N is the Avogadro number, T is temperature in Kelvin and h is Planck's constant. The plots of ln (ν_{corr}/T) versus $1/T$ for the corrosion of the composite in HCl medium of different concentrations are given in the Fig. 7. The enthalpy of activation and entropy of activation were then calculated from the slope and intercept values of the linear plot [29].

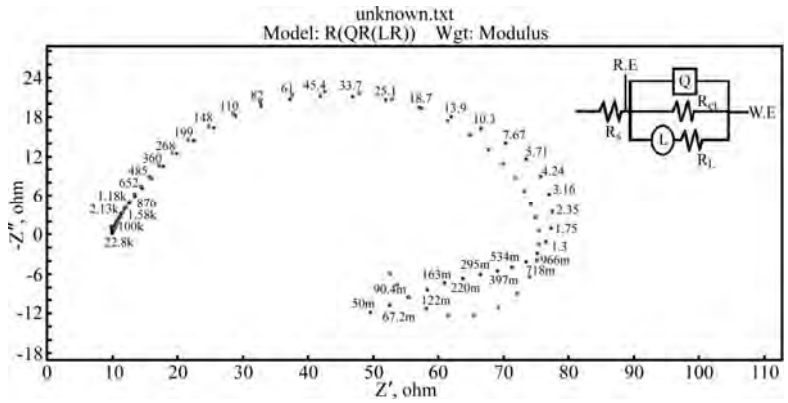

Fig. 3. Simulation plot and equivalent circuit (inset) for the corrosion of 6061 Al-15 vol. pct. $SiC_{(p)}$ composite in 0.1M HCl at 40°C.

Table 3. EIS data for the corrosion of 6061 Al-15 vol. pct. $SiC_{(p)}$ composite in hydrochloric acid

Concentration (M)	Temp (°C)	R_p (Ω·cm^2)	Y_0 (μF·cm^{-2})	n
0.025	30	308.7	55.0	0.78
	35	119.0	119.6	0.80
	40	64.6	180.4	0.80
	45	51.2	251.9	0.80
	50	48.6	260.2	0.75
0.05	30	228.6	67.5	0.80
	35	113.5	129.8	0.80
	40	57.1	181.0	0.80
	45	45.6	280.4	0.80
	50	42.3	291.1	0.76
0.1	30	213.7	83.3	0.80
	35	100.2	136.5	0.80
	40	55.4	201.3	0.80
	45	41.3	343.2	0.80
	50	21.1	565.1	0.78
0.125	30	173.4	89.3	0.80
	35	71.8	153.6	0.80
	40	53.3	210.4	0.80
	45	33.9	351.2	0.80
	50	17.2	601.1	0.80
0.25	30	126.3	107.8	0.80
	35	71.6	177.8	0.80
	40	51.4	231.4	0.80
	45	21.8	413.8	0.80
	50	11.7	509.3	0.80

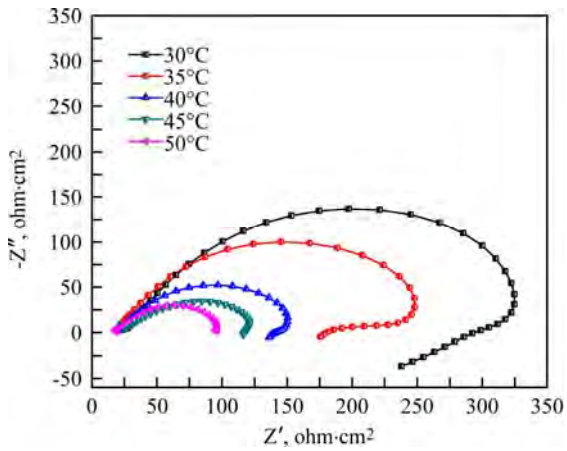

Fig. 4. Nyquist plots for the corrosion of 6061 Al-15 vol. pct. $SiC_{(p)}$ composite in 0.05M HCl at different temperatures.

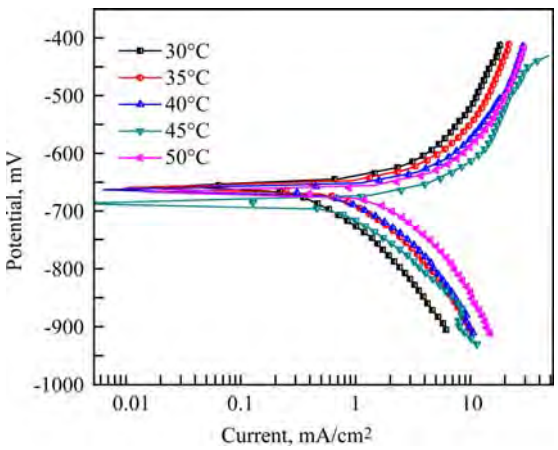

Fig. 5. Potentiodynamic polarization plots for the corrosion of 6061 Al-15 vol. pct. of $SiC_{(p)}$ composite in 0.25M HCl at different temperatures.

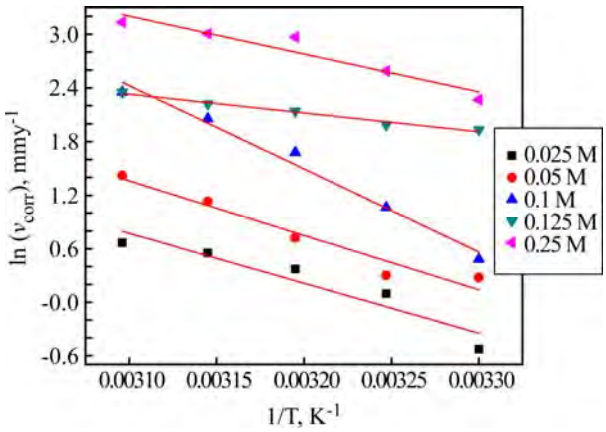

Fig. 6. Arrhenius plots for the corrosion of 6061 Al-15 vol. pct. of $SiC_{(p)}$ composite.

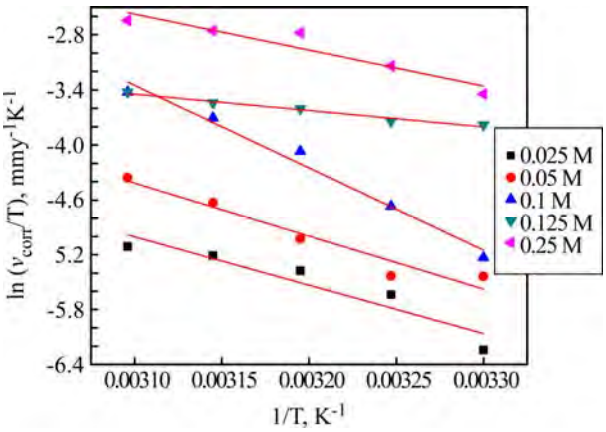

Fig. 7. Plots of ln (v_{corr}/T) versus $1/T$ for the corrosion of 6061 Al-15 vol. pct. of $SiC_{(p)}$ composite.

The Table 4 enlists activation parameters for the corrosion of 6061 Al-15 vol.pct. $SiC_{(p)}$ composite in HCl medium. It is evident from the results presented in the Table that value of activation energy, E_a decreases with the increase in the concentration of the acid, which is confirmatory with the increase in the rate of corrosion. The entropy of activation ($\Delta S^{\#}$) is negative, indicating an association process in the formation of the intermediate activated compound [30–35].

Table 4. Activation parameters for the corrosion of 6061 Al-15 vol. pct. $SiC_{(p)}$ composite

Concentration (M)	E_a (kJ/mol)	$\Delta H^{\#}$ (kJ/mol)	$\Delta S^{\#}$ (J/K/mol)
0.025	46.69	44.09	-102.45
0.05	50.82	48.22	-84.77
0.1	77.37	74.77	-26.88
0.125	17.45	14.85	-180.16
0.25	35.18	32.58	-117.96

Scanning Electron Microscopic Study

The SEM images of the freshly polished sample and the sample immersed in 0.25M HCl for one hour at room temperature are shown in Fig. 8 and Fig. 9, respectively. Figure 8, shows a smooth and even surface and also ceramic SiC reinforced particle whereas Fig. 9 shows rough morphology and the metal dissolution around the reinforced particles is evident. The corrosion appears to be severe around the SiC particles due to the formation of minute electrolytic cell within the restricted area, SiC ceramic acting as cathode and metal acting as anode [22]. The galvanic action triggers the corrosion process.

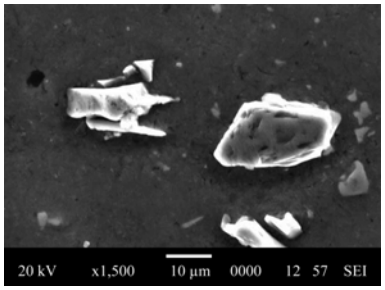

Fig. 8. SEM image of freshly polished surface of 6061 Al-15 vol. pct $SiC_{(p)}$ composite.

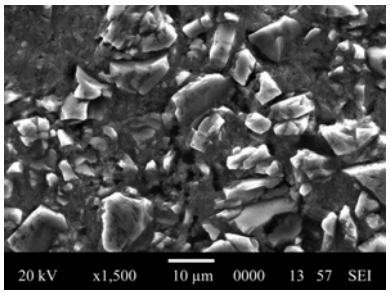

Fig. 9. SEM image of the corroded surface of Al-15 vol. pct. $SiC_{(p)}$ composite.

CONCLUSIONS

A detailed investigation on the corrosion behavior of 6061 Al-15 vol. pct. $SiC_{(p)}$ composite in hydrochloric acid medium of different concentrations and temperatures enabled to draw the following conclusions:

- The corrosion process of the composite is markedly influenced by the environmental parameters like temperature and the HCl concentration.
- Rate of the corrosion increases with the increase in the temperature and acid concentration.
- The kinetics of the corrosion process complies with Arrhenius law.

REFERENCES

1. Soliman H.N. Influence of 8-hydroxyquinoline Addition on the Corrosion Behavior of Commercial Al and Al-HO411 Alloys in NaOH Aqueous Media. *Corros Sci*. 2011, **53**, 2994–3006.
2. Mercier D., Herinx M. and Barthés-Labrousse M.G. Influence of 1, 2-diaminoethane on the Mechanism of Aluminum Corrosion in Sulfuric Acid Solutions. *Corros Sci*. 2010, **52**(10), 3405–3412.
3. Onen A.I., Nwufo B., Ebenso E.E. and Hlophe R.M. Titanium (IV) Oxide as Corrosion Inhibitor for Aluminum and Mild Steel in Acidic Medium. *Int J Electrochem* Sci. 2010, **5**, 1563–1573.
4. Montoya-Dávila M., Pech-Canul M.I. and Pech-Canul M.A. Effect of SiCp Multimodal Distribution on Pitting Behavior of Al/SiC_p Composites Prepared by Reactive Infiltration. *Powder Technol.* 2009, **195**(3), 196–202.

5. Datta J., Samanta B., Jana A., Sinha S., Bhattacharya C. and Bandyopadhyay S. Role of Cl^- and NO^{3-} Ions on the Corrosion Behavior of 20% SiC_p Reinforced 6061-Al Metal Matrix Composite: A Correlation between Electrochemical Studies and Atomic Force Microscopy. *Corros Sci.* 2008, **50**(9), 2658–2668.
6. Candan S. and Bilgic E. Corrosion Behavior of Al–60 vol.% $SiC_{(p)}$ Composites in NaCl Solution. *Mater Lett.* 2004, **58**(22–23), 2787–2790.
7. Aziz I., Zhang Q. and Xiang M. Using EIS to Evaluate Anti-corrosion Properties of the SiCp/5A06 Aluminum MMC Treated by Cerium Conversion Coatings. *J Rare Earth.* 2010, **28**(1), 109–116.
8. Ahmad Z., Paulette P. and Aleem B.A. Mechanism of Localized Corrosion of Aluminum–silicon Carbide Composites in a Chloride Containing Environment. *J Mater Sci*. 2000, **35**(10), 2573–2579.
9. Hamdy A.S., Alfosail F. and Gasem Z. Eco-friendly, Cost-effective Silica-based Protective Coating for an A6092/SiC/17.5p Aluminum Metal Matrix Composite. *Electrochim Acta*. 2013, **89**, 749–755.
10. Kini A., Shetty P., Shetty S.D. and Isloor M.A. Corrosion Inhibition of 6061 Aluminum Alloy/SiC_p Composite in Hydrochloric Acid Medium using 3-chloro-1-benzothiophene-2-carbohydrazide. *Indian J Chem Techn*. 2011, **18**(6), 439–445.
11. Nayak J. and Hebbar K. Corrosion Inhibition of T-6 Treated 6061 Al-$SiC_{(p)}$ Composite in Hydrochloric Acid. *T Indian I Metals.* 2008, **61**(2–3), 221–224.
12. Albiter A., Contreras A., Salazar M. and Gonzalez-Rodriguez J.G. Corrosion Behavior of Aluminum Metal Matrix Composites Reinforced with TiC Processed by Pressure Less Melt Infiltration. *J Appl Electrochem*. 2005, **36**(3), 303–308.
13. Liu X.F., Zhan J. and Liu Q.J. The Influence of Tensile Stress on Electrochemical Noise from Aluminum Alloy in Chloride Media. *Corros Sci*. 2009, **51**(6), 1460–1466.
14. Coleman S., Scott V. and McEnaney B. Corrosion Behavior of Aluminum-based Metal Matrix Composites. *J Mater Sci.* 1994, **29**(11), 2826–2834.
15. Odeshi A.G., Adesola A.O. and Badmos A.Y. Failure of AA 6061 and 2099 Aluminum Alloys under Dynamic Shock Loading. *Eng Fail Anal*. 2013, **35**, 302–314.
16. Al-Turkustani A., Arab S. and Al-Dahiri R. Aloe Plant Extract as Environmentally Friendly Inhibitor on the Corrosion of Aluminum in Hydrochloric Acid in Absence and Presence of Iodide Ions. *Mod Appl Sci*. 2010, **4**(5), 105–124.
17. Kozhukharov S., Kozhukharov V., Schem M., Aslan M., Wittmar M., Wittmar A. and Veith M. Protective Ability of Hybrid Nano-composite Coatings with Cerium Sulfate as Inhibitor Against Corrosion of AA2024 Aluminum Alloy. *Prog Org Coat.* 2012, **73**(1), 95–103.
18. Winkler S.L., Ryan M.P. and Flower H.M. Pitting Corrosion in Cast 7xxx Aluminum Alloys and Fibre Reinforced MMCs. *Corros Sci*. 2004, **46**(4), 893–902.
19. Bhat M., Surappa M. and Nayak H.S. Corrosion Behavior of Silicon Carbide Particle Reinforced 6061/Al Alloy Composites. *J Mater Sci*. 1991, **26**(18), 4991–4996.
20. Khaled K.F. Electrochemical Investigation and Modeling of Corrosion Inhibition of Aluminum in Molar Nitric Acid using Some Sulfur-containing Amines. *Corros Sci*. 2010, **52**(9), 2905–2916.
21. Fontana M.G. *Corrosion Engineering.* New York: Mc Graw Hill, 1986. 739 p.
22. Pinto G.M., Nayak J. and Shetty A.N. Corrosion Behavior of 6061 Al-15 vol. pct. SiCp Composite and its Base Alloy in a Mixture of 1:1 hydrochloric and Sulfuric Acid Medium. *Int J Electrochem Sci.* 2009, **4**, 1452–1468.
23. Pinto G.M., Nayak J. and Shetty A.N. Corrosion Inhibition of 6061 Al–15vol. Pct. SiCp Composite and its Base Alloy in a Mixture of Sulfuric Acid and Hydrochloric Acid by 4-(N,N-dimethyl amino) Benzaldehyde Thiosemicarbazone. *Mater Chem Phys*. 2011, **125**(3), 628–640.
24. Aytaç A., Özmen Ü. and Kabasakaloğlu M. Investigation of Some Schiff Bases as Acidic Corrosion of Alloy AA3102. *Mater Chem Phys*. 2005, **89**(1), 176–181.
25. Behpour M., Ghoreishi S.M., Soltani N., Salavati-Niasari M. Hamadanian M. and Gandomi A. Electrochemical and Theoretical Investigation on the Corrosion Inhibition of Mild Steel by Thiosalicylaldehyde Derivatives in Hydrochloric Acid Solution. *Corros Sci.* 2008, **50**(8), 2172–2181.
26. Deng S. and Li X. Inhibition by Jasminum Nudiflorum lindl. leaves Extract of the Corrosion of Aluminum in HCl Solution. *Corros Sci*. 2012, **64**, 253–262.
27. Singh A.K., Shukla S.K. and Ebenso E.E. Cefacetrile as Corrosion Inhibitor for Mild Steel in Acidic Media. *Int. J Electrochem Sci*. 2011, **6**(11), 5689–5700.
28. Gomma G.K. and Wahdan M.H. Schiff Bases as Corrosion Inhibitors for Aluminum in Hydrochloric Acid Solution. *Mater Chem Phys*. 1995, **39**(3), 209–213.
29. Khaled K., Mghraby A., Ibrahim O., Elhabib O. and Ibrahim M.A. Inhibitive Effect of Thiosemicarbazone Derivative on Corrosion of Mild Steel in Hydrochloric Acid Solution, *J. Mater. Environ. Sci*., 2010, vol.1, pp. 139–150.
30. Fouda A., Elewady G., El-Askalany A. and Shalabi K. Inhibition of Aluminum Corrosion in Hydrochloric Acid Media by Three Schiff Base Compounds. *Zaštita materijala*. 2010, **51**(4), 205–219.
31. Noor E.A. Evaluation of Inhibitive Action of Some Quaternary N-heterocyclic Compounds on the Corrosion of Al–Cu Alloy in Hydrochloric Acid. *Mater Chem Phys*. 2009, **114**(2–3), 533–541.
32. Kumari P.R., Nayak J. and Shetty A.N. 3-Methyl-4-amino-5-mercapto-1, 2, 4-triazole as Corrosion Inhibitor for 6061 Al Alloy in 0.5M Sodium Hydroxide Solution. *J Coating Technol Res.* 2011, **8**(6), 685–695.

33. Obot I.B. and Obi-Egbedi N.O. Anti-corrosive Properties of Xanthone on Mild Steel Corrosion in Sulphuric Acid: Experimental and Theoretical Investigations. *Curr Appl Phys.* 2011, **11**(3), 382–392.

34. Tao Z., Zhang S., Li W. and Hou B. Corrosion Inhibition of Mild Steel in Acidic Solution by Some Oxo-triazole Derivatives. *Corros Sci.* 2009, **51**(11), 2588–2595.

Received 14.07.14
Accepted 21.11.14

Реферат

Микро-гальваническая коррозия алюминиевого сплава 6061 упрочняемого SiC лишает возможности его использования в кислых средах или при высоких температурах. Поэтому коррозионное поведение композита алюминиевый сплав 6061 с 15%об. SiC в среде HCl при различных температурах изучалась методами измерения электрохимического импеданса и регистрации потенциодинамических поляризационных кривых. Исследования показали, что при увеличении ионной концентрации среды и температуры скорость коррозии увеличивается. Изображения поверхности полированного образца и после его выдержки в коррозионной среде, полученные методом сканирующей электронной микроскопии, показали гладкую и неровную морфологии, соответственно. Параметры активации такие, как энергии активации рассчитывали по кривым Аррениуса. Значения энтропии и энтальпии были получены на основании кривых уравнения теории переходного состояния.

Ключевые слова: 6061 алюминиевый композит, электрохимические методы, кислотная коррозия, упрочнение карбидом кремния.